Baku State University: Journal of Physics & Space Sciences, **2025**, v2 (3), p. 53-62

journal homepage: http://bsuj.bsu.edu.az/en

Review: Integration of $BaTiO_3$ Nanoparticles with Graphene for Multifunctional Applications

Lala R. Gahramanli*, Matanat R. Babayeva

Department of Chemical Physics of Nanomaterials, Faculty of Physics,
Baku State University, Baku, Azerbaijan
Received 27-Jun-2025; Accepted 12-Aug-2025
DOI: https://doi.org/10.30546/209501.101.2025.2.03.025

Abstract

This study focuses on the development and application of a hybrid nanocomposite system based on barium titanate ($BaTiO_3$) nanoparticles and graphene nanoplates, targeting its integration into advanced nanoscale devices. The multifunctional nature of $BaTiO_3$, with its well-known ferroelectric and piezoelectric properties, combined with the exceptional electrical conductivity, mechanical strength, and large surface area of graphene, makes this composite highly promising for a range of emerging technologies. In particular, the researchers explored the potential of $BaTiO_3$–graphene nanocomposites in ultrathin piezoelectric resonators, nanogenerators, and surface plasmon resonance (SPR) biosensors. The synergistic interaction between the dielectric and conductive components enhances the overall sensitivity, energy conversion efficiency, and signal transduction capability of the composite. The study further examined the structural integration, stability, and performance of the nanocomposite under various operational conditions, offering insight into its suitability for next-generation micro- and nanoelectromechanical systems (MEMS/NEMS), energy harvesting devices, and high-sensitivity biosensing platforms.

Keywords: barium titanate, graphene nanoplates, piezoelectric resonators, sensors, application field
PACS Numbers: 81.07.-b

1. Introduction

The integration of multifunctional nanomaterials has become essential for advancing next-generation energy and sensing technologies. $BaTiO_3$, a well-established ferroelectric and piezoelectric ceramic, offers excellent dielectric and elec-

*Corresponding author – Tel: (+994) 50 353 61 31
e-mail: gahraman.lala@gmail.com; *ORCID ID*: 0000-0002-3799-8578.

tromechanical properties. Graphene, with its exceptional electrical conductivity, mechanical strength, and high surface area, serves as an ideal counterpart in hybrid nanocomposites. The combination of $BaTiO_3$ nanoparticles with graphene enables the development of materials with enhanced performance suitable for ultrathin piezoelectric resonators, nanogenerators, and SPR biosensors. This study investigates the structural, optical, and functional properties of $BaTiO_3$–graphene nanocomposites and their potential in multifunctional device applications.

2. Discussion

Martin Lee et al. [1] have reported on the application of free-standing complex oxide, $BaTiO_3$ (BTO), and graphene in a piezoelectric resonator, which is considered a crucial element in future telecommunication systems and next-generation electronics. Free-standing thin film bulk acoustic resonators (FBAR) have been embraced as the filter technology for 5G bands [2]. FBAR filters are composed of a thin piezoelectric material inserted between two electrodes. However, to increase the resonance frequency, the thickness of these resonators needs to be reduced. To remove some of these drawbacks, researchers have investigated the free-standing single-crystal $BaTiO_3$ in thin film form with a high piezoelectric coefficient, which can operate at higher voltages and power density. At the same time, the size of electrodes needs to be reduced to meet the requirements of the telecommunication frequencies, which should be able to hold up high-GHz frequencies [3]. In this case, graphene becomes a more suitable electrode material that could conduct electricity down to the single atomic layer. To prepare the free-standing BTO, firstly, a thick crystalline sacrificial layer of $Sr_2Al_3O_6$ (SAO) is deposited onto a TiO_2-terminated $SrTiO_3$(001) [4]. After this process, they grow a high-quality BTO on the SAO layer. The water-soluble property of SAO helps to separate the BTO from the substrate after the shedding in water. Then, the BTO sample is submerged under the water for one day after attaching it with the PDMS (polydimethylsiloxane) to free the SAO layer. After observing the ferroelectricity of the free-standing BTO, it can be used in the capacitor geometry, together with the graphene electrodes. As shown in Figure 1a (graphene layers outlined in dashed black lines and BTO in dashed green lines), firstly, the bottom graphene layer of a thickness of 16 nm is placed over a cavity using the PDMS transfer method in SiO_2/Si, then, a BTO film is added onto the placed graphene layer. Ultimately, a top graphene layer with a thickness of 5 nm is transferred using again PDMS method. Therefore, this heterostructure assembling the sandwiches of graphene and BTO membranes consists of asymmetric graphene layers to block the electric field coming from the top layer to avoid the extra movement caused by this electric field. The bending of the graphene-BTO-graphene heterostructure is defined at room temperature at a pressure of 10^{-5} mbar with the method of a laser interferometry setup. This setup provides

three actuation methods (Figure 1 b-d).

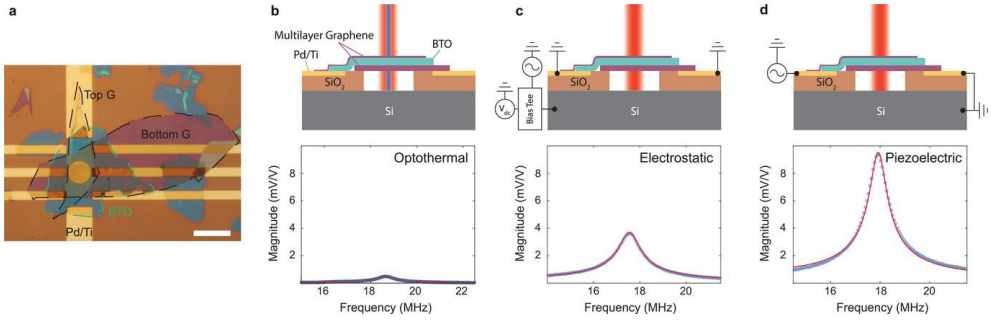

Figure 1. Device geometry and comparison of actuation methods. a) Optical microscopy image of device 1. Top graphene is 5 nm, bottom graphene is 16 nm and BTO is 36 u.c. (≈14.7 nm) thick. Scalebar: 10 µm. b–d) Illustration of the actuation method on top and measured resonance peak using the corresponding actuation method with a 100 mV driving amplitude on the bottom. b) Optothermal driving using an intensity modulated blue (λ = 405 nm) laser with a power of 93 µW. c) Electrostatic driving with Si substrate while grounding the top and bottom graphene. There is no electric field across the BTO. A DC bias voltage of V_{DC} = −1 V is added to V_{AC} using a bias tee. d) Piezoelectric actuation with AC voltage applied to the top graphene while grounding the bottom graphene and the substrate. A red laser (λ = 633 nm) with a power of 2 mW is used in all three measurements to detect displacements [1].

There is no electric field across the BTO. A DC bias voltage of V_{DC} = −1 V is added to V_{AC} using a bias tee. d) Piezoelectric actuation with AC voltage applied to the top graphene while grounding the bottom graphene and the substrate. A red laser (λ = 633 nm) with a power of 2 mW is used in all three measurements to detect displacements [1].

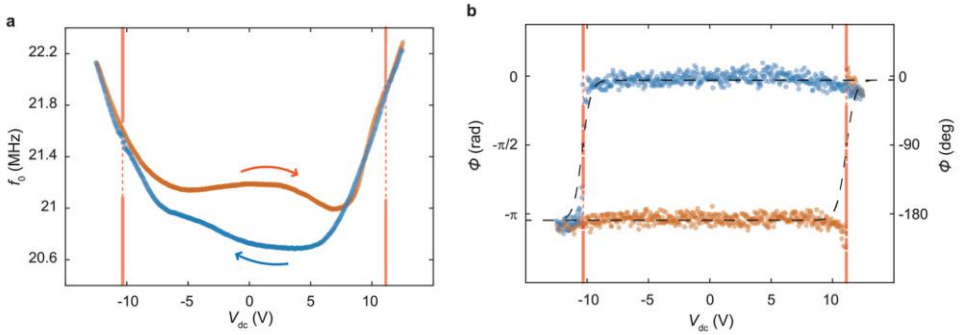

Figure 2. Ferroelectric hysteresis observed in the mechanical observables during a VDC sweep (red and blue data correspond to upward and downward sweep respectively). a) Fundamental resonance frequency f0. b) Phase φ when driving at resonance and a hyperbolic tangent (black dashed lines) fit.

Researchers have focused on the piezoelectric actuation because of its advantages, such as the potential of the readout method. Only in the case of piezoelectric driving, it can be observed that hysteresis occurs in f_0 (resonance frequency), ϕ (phase), and Q factor.

As a conclusion, researchers have demonstrated that ultrathin piezoelectric resonators using SAO layer, to increase the quality of BTO free-standing layer as well as to allow the release of this layer from the substrate without any spoil, and SiO_2/Si, to supply the thermal isolation and to lay out low dielectric loss of the device, have wide range applications in the next-generation telecommunication systems.

Kwi-Park and colleagues [5] have investigated the flexible nanocomposite generator made of $BaTiO_3$ nanoparticles and graphitic carbon. Renewable energy sources, including wind energy [6], solar energy [7, 8], and wave energy [9, 10], can provide the large-scale requirements of global energy, but for driving small electronics, innovative approaches have to be developed. From that perspective, the authors report the nanocomposite generator (NCG) using $BaTiO_3$ NPs [11] and carbon nanomaterials such as single-walled and multi-walled carbon nanotubes (SW/MW-CNTs) as well as reduced graphene oxide dispersed in polydimethylsiloxane (PDMS) by mechanical mixing to achieve the low-cost and large area fabrication. For fabrication, firstly, researchers have used radio frequency magnetron sputtering to deposit the layers of Cr (10 nm) and Au (100 nm) onto the flexible substrates. This process is followed by the spin-casting of a layer of PDMS onto deposited Cr/Au/plastic substrates to form a dielectric layer. To produce a piezoelectric nanocomposite (p-NC), $BaTiO_3$ NPs are mixed with the graphitic carbon in required proportions. After stringing in ethanol and drying in the oven, the compositions of nanomaterials are deposited in a PDMS matrix to obtain the final piezoelectric nanocomposite. This p-NC is spin-cast onto PDMS/Au/Cr/plastic substrates for 30 sec and cured for 5 min in an oven. Finally, another top PDMS/metal-coated plastic substrate is placed onto the deposited bottom flexible substrate to produce the NCG device (Figure 3a). Based on the magnified cross-image taken with the SEM, we can say that $BaTiO_3$ NPs as well as MW-CNTs are well dispersed in the PDMS matrix (Figure 3b and 3c).

Researchers have measured the generated outcomes of the NCG device during the periodic bending and unbending motion of the bending stage (Figure 4). To prove that these signals are only provided by the NCG device, the measurements are conducted according to forward (positive output pulses are received) and reverse connection (negative output pulses recorded) states (Figure 2b-i and ii;2c-i and ii). Under these repeated bending and unbending cycles, the NCG device generates an open-circuit voltage (V_{oc}) of ∼3.2 V and short-circuit current (I_{sc}) of 250 to 350 nA. The contribution of CNTs to the NCG device was very important. CNTs provide a well-distributed distribution of $BaTiO_3$, resulted in high output pulses, reinforcing the stress applied to NPs by enhancing the mechanical properties of composite materials, reducing the internal resistance [12, 13]. Researches have been

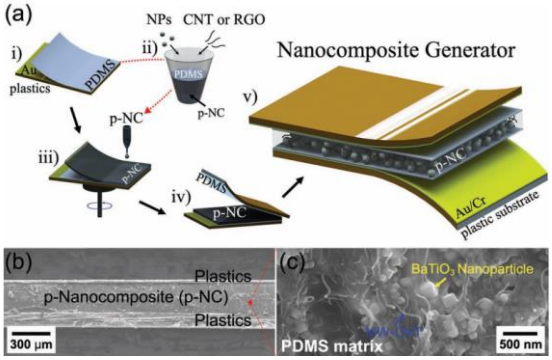

Figure 3. a) Schematic illustration of the process for fabricating NCG device. (b) A crosssectional SEM image of an NCG device. (c) A magnified cross-sectional SEM photograph of the p-NC.

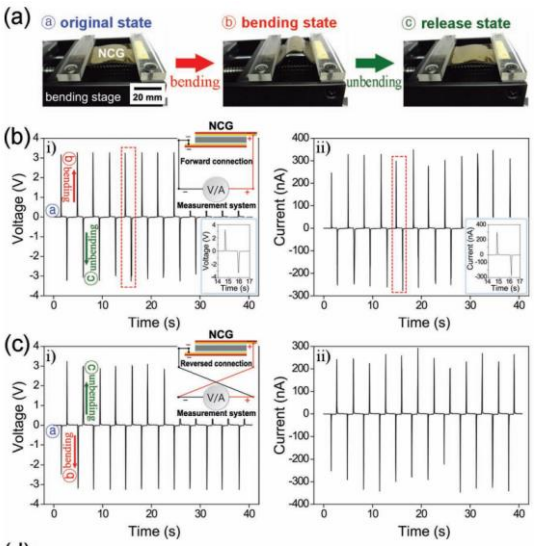

Figure 4. (a) Optical images of NCG devices in their original, bending, and release states. (b) The measured output voltage and current signals of the NCG device in the forward connection during the periodic bending and unbending motions. (c) The open-circuit voltage and short-circuit current signals are generated in the reverse connection [5].

concluded that NCG device utilizing Cr layer, to provide strong adhesion between plastic substrate and Au electrodes, prevent cracking of electrodes by enhancing mechanical robustness, $BaTiO_3$ and graphitic carbon (SW and MW CNTs) is future promising because of enhanced piezoelectric properties, large fabrication area, flexible structure, higher level of power density.

In another study, according to the ideas of N. Mudgal et al., the SPR biosensors based on $BaTiO_3$-graphene-affinity layer have advanced applications in medicine,

including bacterial detection of Pseudomonas species widely found in nature that are the major causes of many infections in humans through contaminated water and food [14, 15, 16]. Generally, in SPR-based biosensors, SPs are generated at the interface of a metal-dielectric surface due to the charge density oscillations of free electrons, and this phenomenon is known as surface plasmon resonance. The low sensitivity of conventional prism-based SPR biosensors with a single metal creates a need for more advanced sensitivity and detection accuracy. The Pseudomonas bacterial attachment to the affinity layer is an important phenomenon for sensing. Also, nanomaterials, including graphene, have been widely used in sensing technology due to their large surface area to volume ratio, physical and structural characteristics. Recently, high refractive index, low dielectric losses, and high dielectric constant of $BaTiO_3$ have been considered as a promising material for biosensors [17, 18]. The high molecule binding ability of the Ag layer enhances the performance of SPR sensors [19, 20, 21]. In this case, researchers have used a $BaTiO_3$ layer between the silver and graphene layers: three affinity layers called nicotine, toluene, and poly (trifluoroethyl methacrylate) for detection in the proposed structure, as illustrated in Figure 5a.

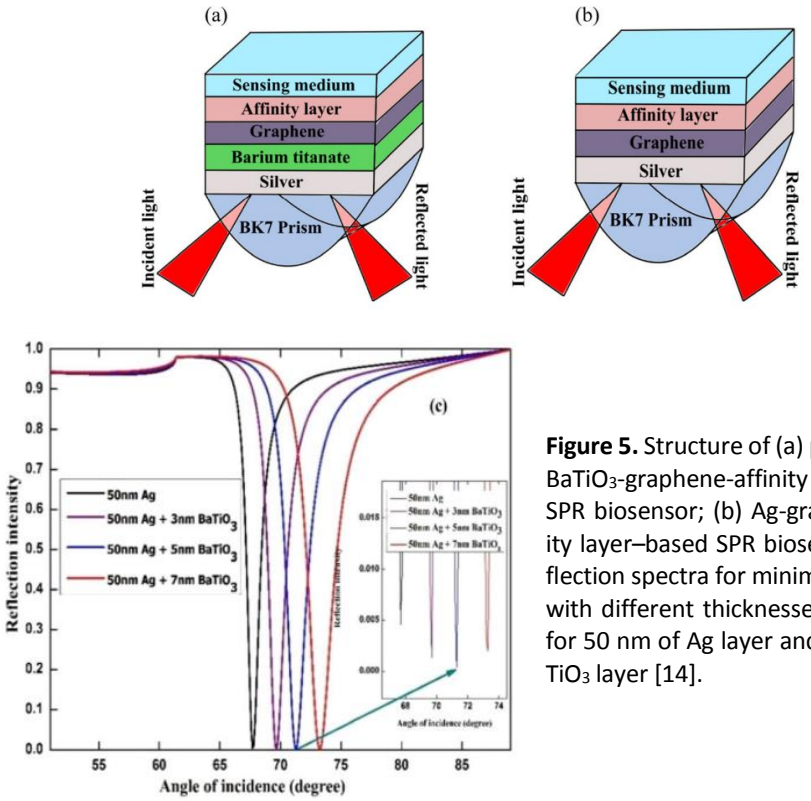

Figure 5. Structure of (a) proposed Ag-$BaTiO_3$-graphene-affinity layer–based SPR biosensor; (b) Ag-graphene-affinity layer–based SPR biosensor; (c) Reflection spectra for minimum intensity with different thicknesses of Ag layer for 50 nm of Ag layer and 5 nm of $BaTiO_3$ layer [14].

In their design, researchers have used a BK7 glass prism with n_{BK7}= 1.5152 [22] to couple the light and He-Ne laser of λ = 633 nm. The design consists of silver as a filet layer having a thickness of 50 nm and n_{Ag}= 0.056206 + 4.2776 [23]. Secondly, the layer of $BaTiO_3$ is deposited on the first layer, having d_{BaTio3} = 5nm and n_{BaTiO3} = 2.4042 [24]. Then, the third layer of graphene with a thickness of 0.34 nm is deposited. The fourth layer is affinity layers with a thickness of 3 nm and three various values of refractive index, i.e., 1.5265 (nicotine), 1.49368 (toluene), and 1.4370 [poly (trifluoroethyl methacrylate)] [25]. In the proposed structure, the sensing medium is chosen as water with n_{water} = 1.33. Generally, the refractive index of the sensing medium changes between 1.33 and 1.40. Note that Figure 1b shows the SPR biosensor without the $BaTiO_3$ layer, where all parameters have the same values as in the discussed SPR biosensor with the $BaTiO_3$ layer. The performance of a sensor can be characterized by the sensitivity, quality parameter, and sensor accuracy. Here, researchers have investigated the effect of the thickness of both silver and $BaTiO_3$ layer for minimum reflectivity at a fixed λ = 633 nm and have found the optimum values of thickness of the and $BaTiO_3$ layers as 50 nm and 5 nm respectively for the graphene layer of thickness 0.34 nm and sensing medium 1.33 as illustrated in Figure 5c. Maximum sensitivity, quality parameter, and detection accuracy for this proposed structure have been defined as 220°/RIU, 101.38 RIU^{-1}, and 7.09, respectively, for the range of n between n = 1.33 to 1.44 for the affinity layer [poly (trifluoroethyl methacrylate)] (Figure 6a). Researchers have also defined the effect of the increasing number of graphene layers and investigated that as this number increases, the minimum reflectivity intensity also increases. Hence, it is the best choice to use the monolayer of graphene for the absorption of Pseudomonas bacteria (Figure 6b).

As a result, the performance of SPR sensor improves with the proposed structure and this design effectively finds its application in the detection of Pseudomonas bacteria.

3. Conclusion

In conclusion, the integration of functional materials such as $BaTiO_3$, graphene, and CNTs has opened new avenues for the development of high-performance ultrathin piezoelectric resonators, NCG devices, and SPR biosensors. The incorporation of a sacrificial SAO layer and thermal isolation SiO_2/Si substrates has been shown to enhance the quality and performance of free-standing $BaTiO_3$ layers, making them highly suitable for next-generation telecommunication systems. In NCG devices, the use of CNTs significantly improves the mechanical robustness, stress distribution, and electrical output, leading to open-circuit voltages of ∼3.2 V and current levels up to 350 nA during mechanical deformation cycles. Additionally, the optimized design of SPR biosensors using $BaTiO_3$ and monolayer graphene has demon strated high sen-

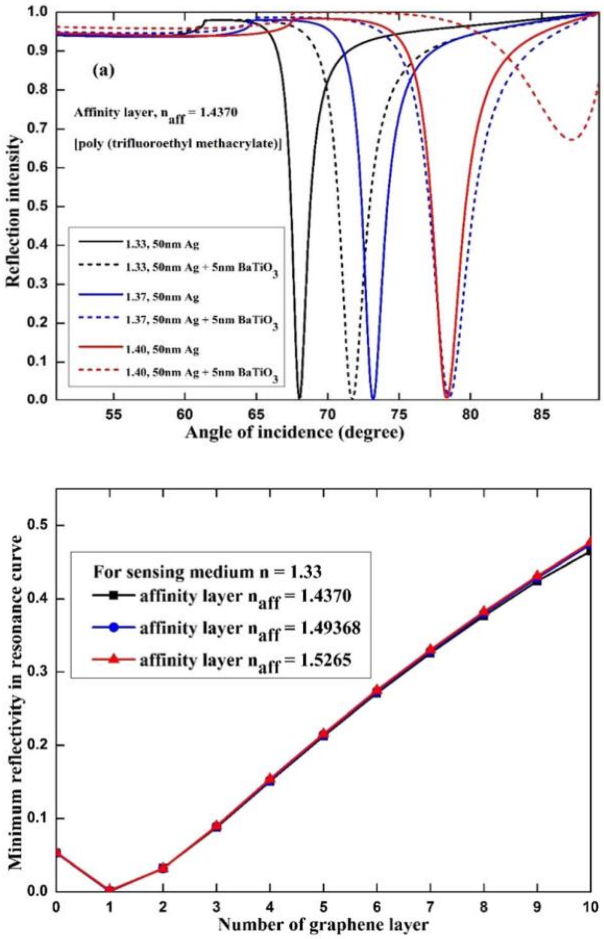

Figure 6. (a) Reflection spectra of the proposed structure (dash line) having thicknesses of dAg = 50 nm, d_{BaTiO3} = 5 nm, and dGraphene = 0.34 nm, and structure without BaTiO3 layer (solid line) having thicknesses of d_{Ag} = 50 nm and $d_{Graphene}$ = 0.34 nm and sensing medium of refractive index 1.33 for affinity layer of refractive index n_{aff} = 1.4370 [poly (trifluoroethyl methacrylate)]; (b) Plot of minimum reflectivity with number of graphene layer with thickness of d_{Ag} = 50 nm, d_{BaTiO3} = 5 nm, $d_{graphene}$ = 0.34 nm (monolayer), and d_{aff} = 3 nm and sensing medium of refractive index 1.33 [14].

sitivity (220°/RIU), quality factor (101.38 RIU^{-1}), and accuracy (7.09), particularly in detecting biomolecules like Pseudomonas bacteria. Overall, these findings affirm that $BaTiO_3$-based nanocomposites, when strategically integrated with carbon nanomaterials and optimized device architectures, hold strong promise for multifunctional, flexible, and high-sensitivity applications in energy harvesting, sensing, and biomedical diagnostics.

References

[1] Lee, M., Renshof, J. R., van Zeggeren, K. J., Houmes, M. J. A., Edouard, L., Makars, Š., van Thiel, T. C., Guis, R. H., van Blankenstein, M. R., Verbiest, G. J., Caviglia, A. D., van der Zant, H. S. J., & Steeneken, P. G. (2022). Ultrathin piezoelectric resonators based on graphene and free-standing single-crystal BaTiO3. *Advanced Materials, 34*(37), 2204630. https://doi.org/10.1002/adma.202204630

[2] Liu, Y., Cai, Y., Zhang, Y., Tovstopyat, A., Liu, S., & Sun, C. (2020). Micromachines. *Micromachines, 11*(7), 630. https://doi.org/10.3390/mi11070630

[3] Wu, Y., Jenkins, K. A., Valdes-Garcia, A., Farmer, D. B., Zhu, Y., Bol, A. A., Dimitrakopoulos, C., Zhu, W., Xia, F., Avouris, P., & Lin, Y.-M. (2012). *Nano Letters, 12*(6), 3062–3067. https://doi.org/10.1021/nl300904k

[4] Lu, D., Baek, D. J., Hong, S. S., Kourkoutis, L. F., Hikita, Y., & Hwang, H. Y. (2016). *Nature Materials, 15*(12), 1255–1260. https://doi.org/10.1038/nmat4749

[5] Park, K.-I., Lee, M., Liu, Y., Moon, S., Hwang, G.-T., Zhu, G., Kim, J. E., Kim, S. O., Kim, D. K., Wang, Z. L., & Lee, K. J. (2012). Flexible nanocomposite generator made of BaTiO3 nanoparticles and graphitic carbons. *Advanced Materials, 24*(22), 2999–3004. https://doi.org/10.1002/adma.201200105

[6] Roundy, S., Leland, E. S., Baker, J., Carleton, E., Reilly, E., Lai, E., Otis, B., Rabaey, J. M., Wright, P. K., & Sundararajan, V. (2005). Improving power output for vibration-based energy scavengers. *IEEE Pervasive Computing, 4*(1), 28–36. https://doi.org/10.1109/MPRV.2005.14

[7] Priya, S., & Inman, D. J. (2009). *Energy harvesting technologies*. Springer. https://doi.org/10.1007/978-0-387-76464-1

[8] Roundy, S., Wright, P. K., & Rabaey, J. (2003). A study of low level vibrations as a power source for wireless sensor nodes. *Computer Communications, 26*(11), 1131–1144. https://doi.org/10.1016/S0140-3664(02)00248-7

[9] Rhinefrank, K. (2005, April 26–28). *Energy Ocean 2005*. Washington, DC.

[10] Hagerman, G., Scott, G., & Jacobson, P. T. (2011). *Mapping and assessment of the United States ocean wave energy resource* (No. DOE-GO-18173-1). Electric Power Research Institute (EPRI).

[11] Chen, D. R., & Jiao, X. L. (2000). *Journal of the American Ceramic Society, 83*(10), 2637–2640. https://doi.org/10.1111/j.1151-2916.2000.tb01606.x

[12] Suhr, J., Koratkar, N., Keblinski, P., & Ajayan, P. (2005). *Nature Materials, 4*(2), 134–137. https://doi.org/10.1038/nmat1293

[13] Veedu, V. P., Cao, A. Y., Li, X. S., Ma, K. G., Soldano, C., Kar, S., Ajayan, P. M., & Ghasemi-Nejhad, M. N. (2006). *Nature Materials, 5*(6), 457–462.

https://doi.org/10.1038/nmat1656

[14] Mudgal, N., Yupapin, P., Ali, J., & Singh, G. (2020). BaTiO3-graphene-affinity layer–based surface plasmon resonance (SPR) biosensor for Pseudomonas bacterial detection. *Plasmonics, 15*(6), 1581–1590. https://doi.org/10.1007/s11468-020-01146-2

[15] Riveros-Rosas, H., Julian-Sanchez, A., Moreno-Hagelsieb, G., & Munoz Clares, R. A.

(2019). Aldehyde dehydrogenase diversity in bacteria of the *Pseudomonas* genus. *Chemico-Biological Interactions, 304*, 83–87.

https://doi.org/10.1016/j.cbi.2019.03.006

[16] Liu, T., Hou, J., & Peng, Y. (2017). Effect of a newly isolated native bacteria, Pseudomonas NP22, on desulfurization of low-rank lignite. *International Journal of Mineral Processing, 162*, 6–11. https://doi.org/10.1016/j.minpro.2017.02.014

[17] Fouad, S., Sabri, N., Jamal, Z. A. Z., & Poopalan, P. (2017). Surface plasmon resonance sensor sensitivity enhancement using gold–dielectric material. *International Journal of Nanoelectronics and Materials, 10*, 149–158.

[18] Sun, P., Wang, M., Liu, L., Jiao, L., Du, W., Xia, F., Liu, M., Kong, W., Dong, L., & Yun, M. (2019). Sensitivity enhancement of surface plasmon resonance biosensor based on graphene and barium titanate layers. *Applied Surface Science, 475*, 342–347. https://doi.org/10.1016/j.apsusc.2018.12.283

[19] Sharma, A. K., & Pandey, A. K. (2018). Blue phosphorene/MoS_2 heterostructure-based SPR sensor with enhanced sensitivity. *IEEE Photonics Technology Letters, 30*(7), 595–598. https://doi.org/10.1109/LPT.2018.2803747

[20] Gan, S., Zhao, Y., Dai, X., & Xiang, Y. (2019). Sensitivity enhancement of surface plasmon resonance sensors with 2D franckeite nanosheets. *Results in Physics, 13*, 102320. https://doi.org/10.1016/j.rinp.2019.102320

[21] Chen, S., & Lin, C. (2016). High-performance bimetallic film surface plasmon resonance sensor based on film thickness optimization. *Optik, 127*(19), 7514–7519. https://doi.org/10.1016/j.ijleo.2016.05.040

[22] Lin, Z., Jiang, L., Wu, L., Guo, J., Dai, X., Xiang, Y., & Fan, D. (2016). Tuning and sensitivity enhancement of surface plasmon resonance biosensor with graphene covered Au-MoS2-Au films. *IEEE Photonics Journal, 8*(6), 1–8.

https://doi.org/10.1109/JPHOT.2016.2631407

[23] Johnson, P. B., & Christy, R. W. (1972). Optical constants of the noble metals. *Physical Review B, 6*(12), 4370–4379. https://doi.org/10.1103/PhysRevB.6.4370

[24] Wemple, S. H., Didomenico, J. M., & Camlibel, I. (1968). Dielectric and optical properties of melt-grown BaTiO3. *Journal of Physics and Chemistry of Solids, 29*(10), 1797–1803. https://doi.org/10.1016/0022-3697(68)90164-9

[25] Kushwaha, A. S., Kumar, A., Kumar, R., Srivastava, M., & Srivastava, S. K. (2018). Zinc oxide, gold, and graphene-based surface plasmon resonance (SPR) biosensor for detection of Pseudomonas-like bacteria: A comparative study. *Optik, 172*, 697–707. https://doi.org/10.1016/j.ijleo.2018.07.066